Annamraju and Nandiraju *Protection and Control of Modern Power Systems* (2019) 4:16
https://doi.org/10.1186/s41601-019-0130-8

Protection and Control of Modern Power Systems

ORIGINAL RESEARCH Open Access

Robust frequency control in a renewable penetrated power system: an adaptive fractional order-fuzzy approach

Anil Annamraju* and Srikanth Nandiraju

Abstract

Purpose: Load frequency control (LFC) in today's modern power system is getting complex, due to intermittency in the output power of renewable energy sources along with substantial changes in the system parameters and loads. To address this problem, this paper proposes an adaptive fractional order (FO)-fuzzy-PID controller for LFC of a renewable penetrated power system.

Design/methodology/approach: To examine the performance of the proposed adaptive FO-fuzzy-PID controller, four different types of controllers that includes optimal proportional-integral-derivative (PID) controller, optimal fractional order (FO)-PID controller, optimal fuzzy PID controller, optimal FO-fuzzy PID controller are compared with the proposed approach. The dynamic response of the system relies upon the parameters of these controllers, which are optimized by using teaching-learning based optimization (TLBO) algorithm. The simulations are carried out using MATLAB/SIMULINK software.

Findings: The simulation outcomes reveal the supremacy of the proposed approach in dynamic performance improvement (in terms of settling time, overshoot and error reduction) over other controllers in the literature under different scenarios.

Originality/value: In this paper, an adaptive FO-fuzzy-PID controller is proposed for LFC of a renewable penetrated power system. The main contribution of this work is, a maiden application has been made to tune all the possible parameters of fuzzy controller and FO-PID controller simultaneously to handle the uncertainties caused by renewable sources, load and parametric variations.

Keywords: Adaptive fractional order-fuzzy-PID controller, Renewable energy sources, Load frequency control, TLBO algorithm

1 Introduction

In today's modern power systems, the increased electrical energy demand from conventional power sources is becoming expensive and also environmentally hazardous, especially for remote locations and islands. To address these issues, renewable energy sources (RES) would be an attractive alternative solution to meet energy requirements. These RES are clean, but are volatile in nature [1] and this volatility of RES introduces new technical challenges with respect to secure operation of the grid, particularly in frequency control [2]. In order to ensure frequency stability, vast-scale energy storage systems (ESSs) have become a vital part in a RES penetrated interconnected power system [3, 4]. Among all ESSs, plug-in hybrid electric vehicles (PHEVs) form an excellent option for frequency stability studies due to its inherent distributed availability, fast-acting capability and a slow discharge rate while in the idle condition [5, 6]. Moreover, the PHEVs could be utilized by consumers to meet their travel needs, in view of their low-cost charging, reduced CO_2 emissions and fossil fuel usages.

* Correspondence: ani223kumar@gmail.com
Department of Electrical Engineering, National Institute of Technology Warangal, Warangal, Telangana 506004, India

During the last decade, the PHEVs are being considered by several authors for their proposed load frequency control (LFC) studies with various controllers [7–19]. In [7] authors suggested a conventional PI/PID controller, in [8] an adaptive control method, in [9] authors proposed a robust PI controller, in [10] a coefficient diagram method, in [11] a generalized model predictive controller (MPC), in [12] with H_∞ controller, etc. In [13–17] the authors proposed various optimization techniques for secondary LFC with PHEVs. In [13] with a PSO optimized PID controller, in [14] with an imperialistic competitive algorithm (ICA), in [15] with flower pollination algorithm (FPA), in [16] with the whale optimization algorithm, in [17] with the sine-cosine algorithm (SCA), etc. In [15–17], the authors added the fractional-order feature to PID controllers to enhance the system frequency deviation response with RES and PHEVs. In [18, 19], the authors proposed various fuzzy PID controllers. In [18] authors suggested traditional fuzzy PID controller, in [19] the authors proposed FO-Fuzzy-PID controller.

All the above-discussed strategies are applied on linear power systems and have not considered the possible nonlinearities like boiler dynamics, governor dead-band, turbine reheat mechanism, and generator rate constraint (GRC) simultaneously in the conventional power sources. The communication delays in EVs have also not been considered. In addition to the above-mentioned nonlinearities, the intermittent nature of RES along with reduced system inertia changes the system operating conditions extensively [20]. In order to handle all the above-said difficulties, the power system urges an intelligent and efficient controller. From the literature, fractional-order (FO) and fuzzy logic controllers (FLC) are proven as efficient controllers to address the non- linearities in the system.

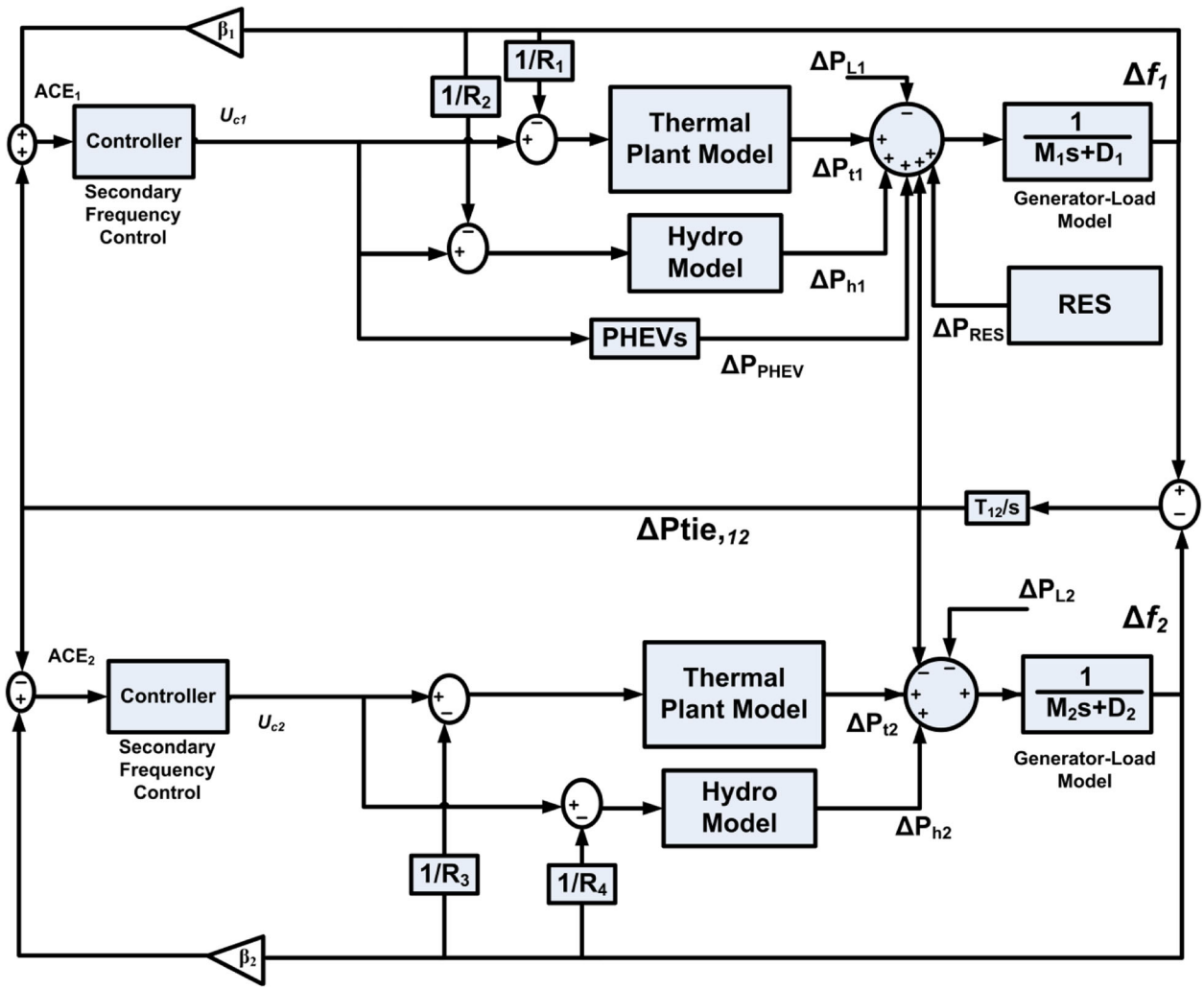

Fig. 1 Two-area power system model

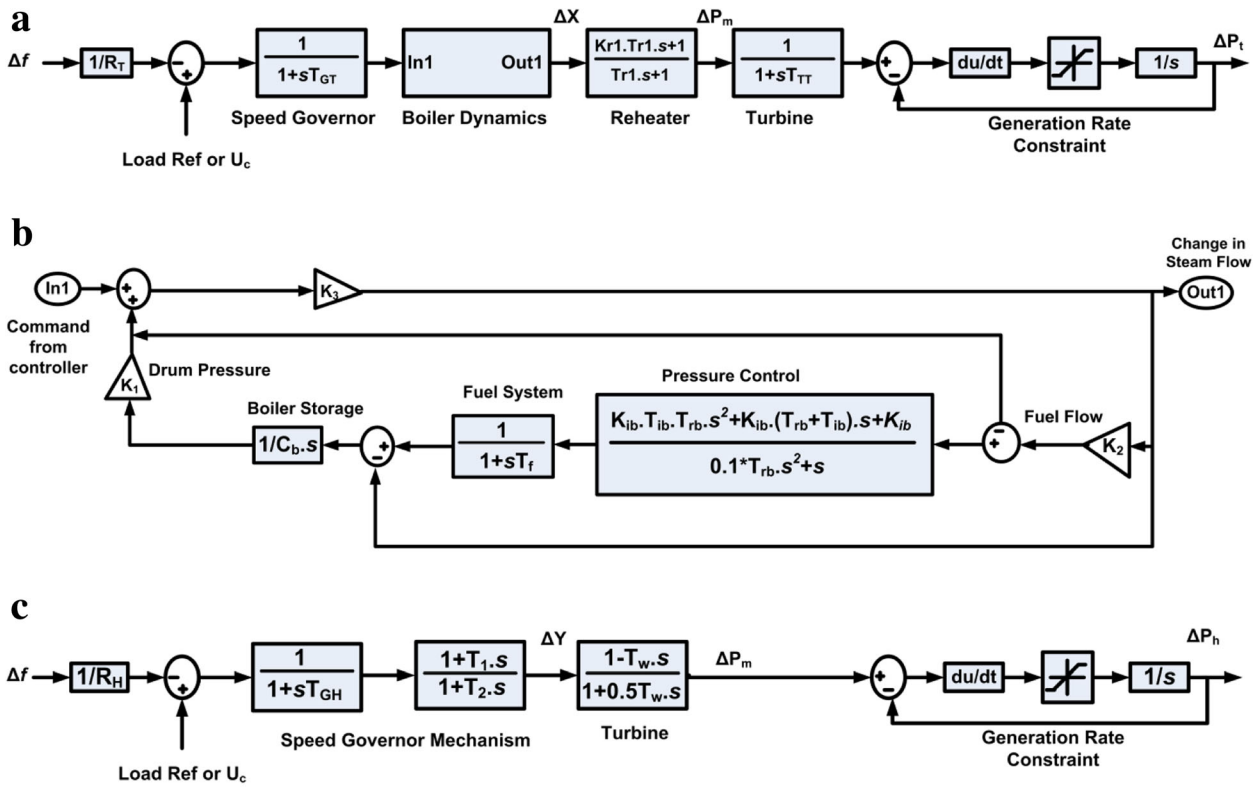

R_T,R_H: Droop coefficient of thermal and hydro unit; T_{GT},T_{GH}: Governor time constant of thermal and hydro unit; T_{rt}: Turbine reheat time constant; K_{rt}: Coefficient of re-heat; T_{TT}: Time constant of steam turbine; ΔP_m: change in mechanical power; ΔP_t: change in output power of thermal unit; T_1:Hydro governor rest time; T_2:Transient droop time constant; T_W: Water time constant; T_{TH}: Time constant of turbine; ΔP_m: change in mechanical power; ΔP_H: change in output power of thermal unit

Fig. 2 Mathematical model of **a** thermal unit, **b** boiler dynamics and **c** Hydro unit

However, it is also noticed that the FO controllers are model dependent and provide better performance only when the exact mathematical model is available. The aforementioned drawback of FO controllers can be overcome by employing FLC. However, their performance highly depends on the optimal selection of membership functions (MFs) and rule base [21]. In order to overcome the specified problems, this paper proposes a novel adaptive FO-fuzzy-PID controller for frequency control of the power system by inheriting the merits of both FL and FO controllers. In this proposed controller, the parameters of FLC (MFs scaling factors and rule base weights) and FO-

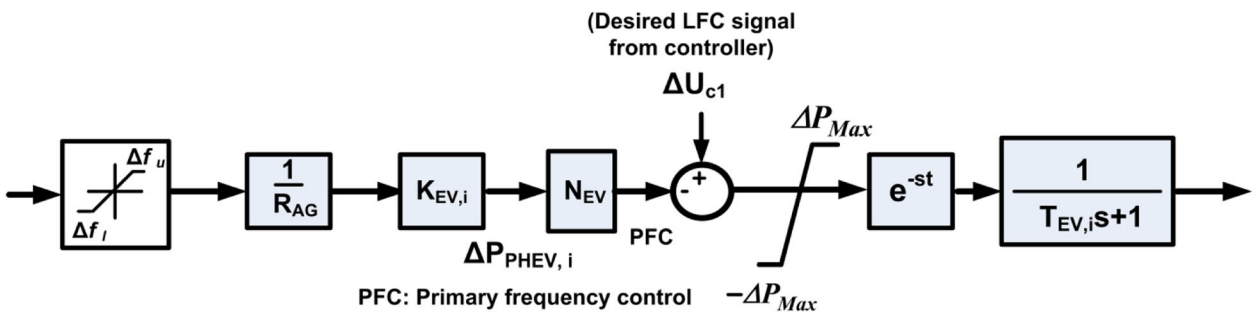

Fig. 3 PHEV aggregator model

PID controller are tuned in online using TLBO algorithm. This algorithm is selected because, unlike other algorithms, it is free from algorithm-specific parameters [22]. The superiority of the proposed controller in terms of dynamic performance over the other controllers (PID/FO-PID/Fuzzy-PID/optimized FO-Fuzzy-PID) in the literature is presented in the Section 5.

The key features of this paper are listed below:

1) An adaptive model free non-linear controller is proposed by integrating the fuzzy logic and fractional order PID controller features to the LFC problem of RES penetrated power system by considering all non-linearities.
2) The FLC performance depends on its MFs scaling factors and rule base weights. A parameter-free optimization (TLBO algorithm) is used for optimal tuning of scaling factors, rule base weights and FO-PID controller parameters.
3) To assess the performance of the proposed controller, an aggregated model of PHEVs with communication delay is also considered in the LFC study
4) Finally, the robustness of the proposed controller is proven by considering various scenarios with parametric uncertainties in single controller framework.

2 Modelling of two-area power system

Figure 1 illustrates a mathematical model of IEE Japan East 107-bus-30-machine power system, which is modelled as a two-area interconnected power system. This test system consists of conventional power sources (CPS), RES and PHEV aggregator. There are two types of CPS in each area which are thermal and hydro generators with an aggregated speed control mechanism. LFC signals (U_{c1}, U_{c2}) are inputted to the governor of each unit. Each turbine output deviation is inputted to the generator-load model and the system frequency deviations (Δf_1, Δf_2) are outputted. In area1, CPS and PHEV aggregator are responsible for generation-load balance, in area2, CPS are only responsible for the generation-load balance. These two areas are interconnected with an AC tie-line with a maximum allowable capacity of 500 MW.

In the interconnected power systems, the difference between schedule and actual generation is defined as area control error (ACE) [23]:

$$\begin{aligned} ACE_1 &= \beta_1 * \Delta f_1 + \Delta P_{tie,12.} \\ ACE_2 &= \beta_2 * \Delta f_2 + \Delta P_{tie,21} \end{aligned} \quad (1)$$

where,

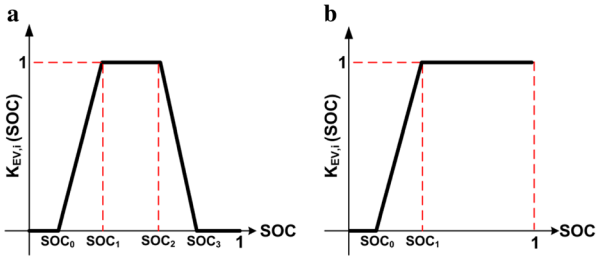

Fig. 4 $K_{EV,\ i}$ vs. SOC **a** Discharge Mode, **b** Idle Mode

$$\Delta f_1 = \frac{1}{M_1 s + D_1}(\Delta P_{t1} + \Delta P_{h1} + \Delta P_{RES} + \Delta P_{PHEV} - \beta_1 \Delta f_1 - \Delta P_{L1});$$

$$\beta_1 = \frac{1}{R_1} + \frac{1}{R_2} + D_1, \Delta f_2 = \frac{1}{M_2 s + D_2}(\Delta P_{t2} + \Delta P_{h2} - \beta_2 \Delta f_2 - \Delta P_{L2});$$

$$\beta_2 = \frac{1}{R_3} + \frac{1}{R_4} + D_2; \Delta P_{tie,12} = \frac{T_{12}}{s}(\Delta f_1 - \Delta f_2) \text{ and } \Delta P_{tie,21} = -\Delta P_{tie,12}$$

Where β_1, β_2 denotes the frequency bias factor of area 1 & area 2; Δf_1, Δf_2 denotes the frequency deviation in area 1 & area 2; T_{12} denotes the synchronizing power coefficient; $\Delta P_{tie,12}$ denotes the tie-line power deviation; U_{c1}, U_{c2} denotes the control signal from controller; ΔP_{PHEV} denotes the change in output power from EV aggregator; ΔP_{RES} denotes the change in output power from renewable sources; ΔP_{L1}, ΔP_{L2} denotes change in a load of area 1 & area 2; ΔP_{t1}, ΔP_{t2} denotes change in the output power of thermal units in area 1 & area 2; ΔP_{h1}, ΔP_{h2} denotes the change in output power of hydro units in area 1 & area 2; M_1, M_2 denotes the equivalent inertia constant of area 1 & area 2; D_1, D_2 denotes the load damping coefficient of area 1 & area 2; ACE_1, ACE_2 denotes the area control error of area1 & area 2.

Finally, the control signal fed to the governors of each area (U_{ci}) can be expressed as:

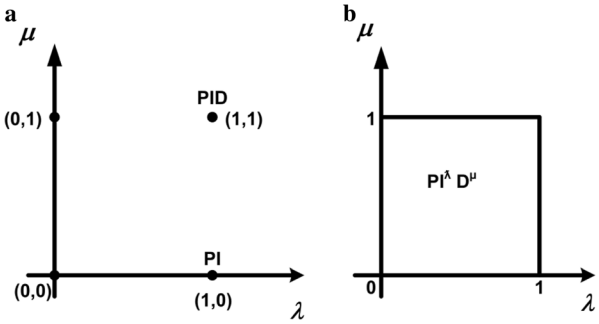

Fig. 5 Representation of controllers in λ-μ plane: **a** IOPID Controller **b** FOPID controller

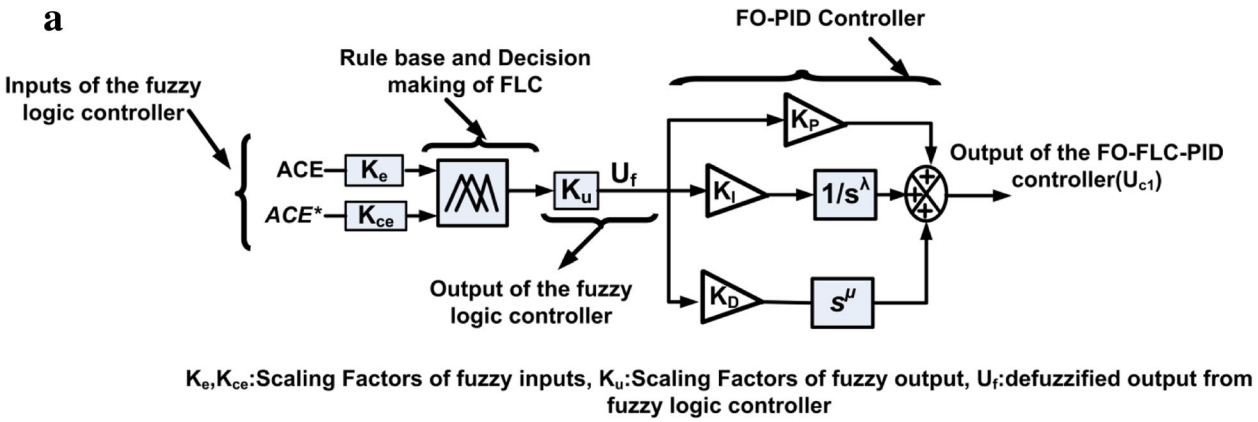

Fig. 6 **a** Structure of FOFPID controller, **b** MFs of inputs & output of FLC

$$U_{ci} = K_p ACE_i + \frac{K_I}{s^{\lambda}} ACE_i + K_D * (s^{\mu} ACE_i) \text{ where i} = 1, 2. \quad (2)$$

Where K_p, K_I, K_D denotes gains of the PID controller and λ, μ denotes the fractional parameters of integrator and differentiator.

The objective of the controller is to minimize the frequency and tie-line power deviations to schedule values by minimizing the ACE.

2.1 Thermal and hydro generator models

Figure 2a-c shows the mathematical models of the thermal generator, boiler dynamics and hydro generator with all possible non-linearities. This model include all appropriates for LFC studies, i.e. speed governor mechanism, boiler dynamics, reheat-turbine system, and generator-load model, etc. [23, 24].

Thermal and hydro generators are responsible for load-generation balance in the system by supplying the deficient power to load depending on RES and PHEV aggregator output power. As shown in Fig. 2a & c, the governors of thermal and hydro units adjust their respective valve positions (ΔX and ΔY) according to the control signal (U_c) in order to meet the load changes. Where ΔP_t and ΔP_h

Table 1 FLC rule base

ACE	ACE*				
	NL	N NM M	N Z S	PME	PLPS
NL	NL	NL	NL	NM	Z
NM	NL	NL	NM	Z	PM
Z	NL	NM	Z	PM	PL
PM	NM	Z	PM	PL	PL
PL	Z	PL	PL	PL	PL

*indicates a change in area control error

indicates the corresponding changes in thermal and hydro generator powers with respect to the load changes.

2.2 PHEVs

In renewable-rich power systems, the volatility in the RES output power along with load changes leads to large excursions in the system frequency. The governors of the hydro and thermal units are not adequate to mitigate the frequency fluctuations due to their sluggish response [20]. So this conventional sources need an additional energy source with immediate response to discharge or store the energy. The quick reaction of PHEVs makes it a significant alternative [25].

Figure 3 depicts the mathematical model of PHEV aggregator. The output power of PHEV for discharging or charging is selected based on the control signal (U_{c1}) from the controller. In the present work, the U_{c1} is determined by using the adaptive fractional-order fuzzy PID controller. A bi-directional vehicle-to-grid (V2G) power control PHEV is chosen for this study. In Fig. 3, the EV aggregator model consists of PFC, LFC and battery charger. e^{-sT} denotes the time delay in the system due to communication delays between LFC control centre and EV aggregator. $T_{EV,\ i}$ denotes the battery time constant; R_{AG} denotes the speed regulation constant of the EV aggregator. $K_{EV,\ i}$ denotes the individual EV's participation factor in the frequency control. The EVs participate in LFC only when they are in charging mode or in idle mode. The participation factor ($K_{EV,\ i}$) of each EV depends on their respective battery SOC level. Figure 4a & b shows the $K_{EV,\ i}$ vs. Battery state-of-charge (soc) of discharge mode and idle mode. If the EVs are disconnected from aggregator, $K_{EV,\ i}$ = 0. Detailed information regarding the aggregated PHEV model and participation factors is available in [25]. ΔP_{PHEV} represents the change in output power of PHEV aggregator. The maximum upward (ΔP_{AG}^{max}) and downward power (ΔP_{AG}^{min}) from the PHEV aggregator can be expressed as:

$$\Delta P_{AG}^{max} = +\left(N_{EV} * \Delta P_{EV,i}\right) \tag{3}$$

$$\Delta P_{AG}^{min} = -\left(N_{EV} * \Delta P_{EV,i}\right) \tag{4}$$

Where N_{EV} represents the number of electric vehicles participating in frequency control. If $\Delta P_{PHEV} > \Delta P_{AG}^{max}$ then $\Delta P_{PHEV} = \Delta P_{AG}^{max}$ and If $\Delta P_{PHEV} < \Delta P_{AG}^{min}$ then $\Delta P_{PHEV} = \Delta P_{AG}^{min}$.

3 Overview of fractional order (FO)& fuzzy logic controllers

3.1 FO-PID controller

Fractional analytics is a standout amongst the essential branches of calculus in which the order of the integral and differential can take a non-integer value. Since a recent couple of decades, the fractional calculus has been applied successfully in numerous fields of engineering.

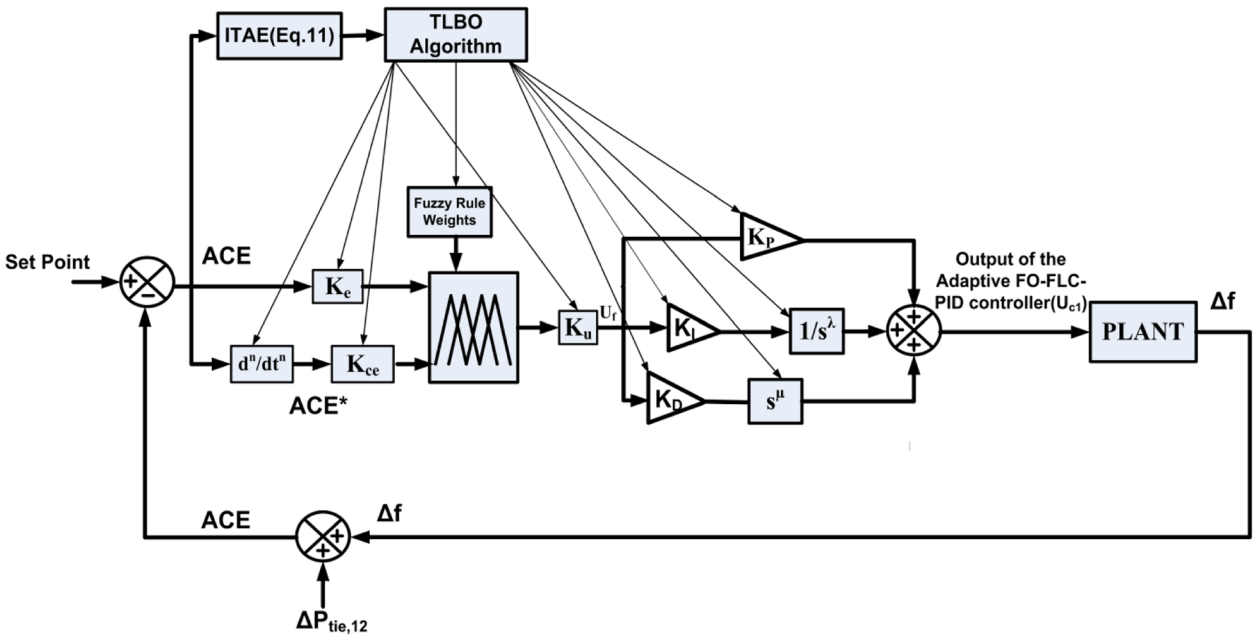

Fig. 7 Structure of proposed adaptive FO-Fuzzy-PID

The detailed analysis regarding fractional calculus is available in [26]. The FO-PID controller can be expressed as:

$$G_c(s) = K_P + \frac{K_I}{s^{\lambda}} + K_D s^{\mu} \tag{5}$$

Where K_P, K_I, and K_D denotes the gains of the proportional, integral and derivative controllers. λ & μ denotes the order of integrator and differentiator. In this FO-PID controller, a total of five variables need to be optimized, three parameters K_P, K_I, and K_D (same as PID) and two fractional parameters λ, μ. These controllers can exhibits better dynamic performance over an integer order PID controllers (IOPID) due to its additional two degrees of freedom in tuning the two additional non-integer knobs (i.e. λ & μ) [27]. In Eq. (5), if (λ, μ) = (0,0) then it becomes the proportional controller; if (λ, μ) = (1,0) then it becomes PI controller; if (λ, μ) = (0,1) then it becomes PD controller; if (λ, μ) = (1,1) then it becomes PID controller. Figure 5a illustrates the various IOPID controllers in the λ-μ plane. Figure 5b shows the realization of FO-PID controller from the integer order PID controller which expands it from the entire λ-μ plane [19, 27].

3.2 FO-fuzzy-PID controller

Figure 6a illustrates the structure of the FO-Fuzzy-PID controller. The inputs of the controller are ACE, ACE* and output is U_f. Fuzzy logic approach can be

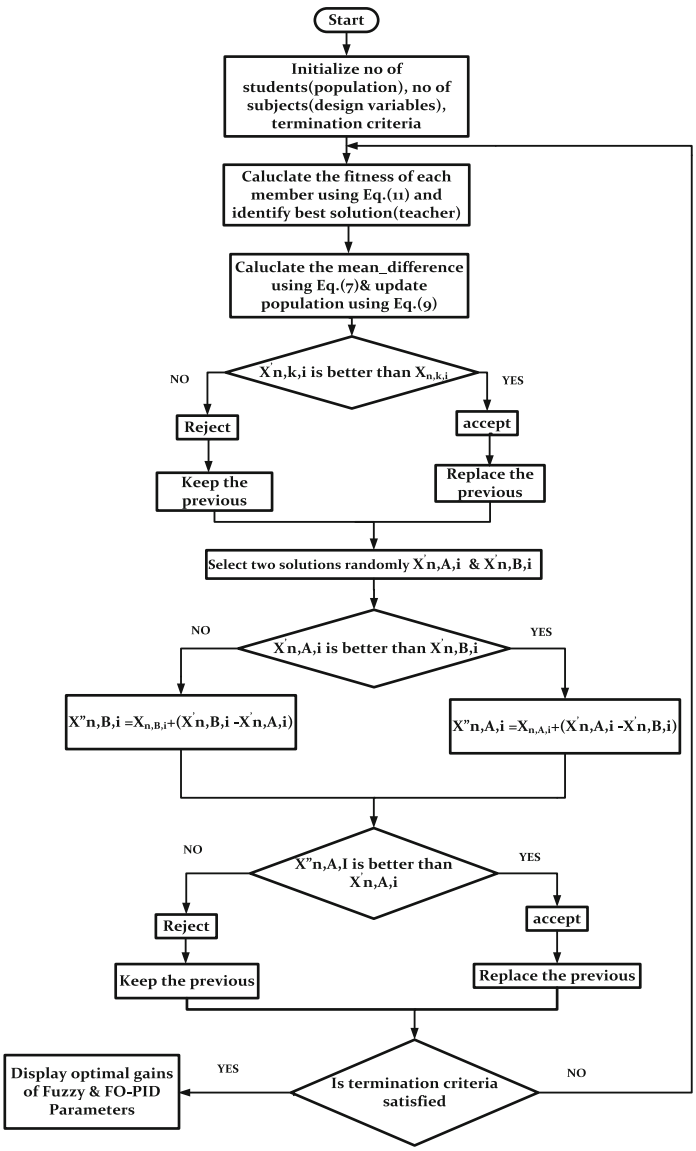

Fig. 8 Flow chart for the tuning of proposed controller with TLBO algorithm

divided into three modules viz. fuzzifier, inference engine and the defuzzifier. The fuzzifier assigns the MF ranges to the input and output variables. Figure 6b depicts the MF ranges corresponding to the inputs and output variables which are arranged as Negative Large (NL), Negative Medium (NM), Zero (ZE), Positive Medium (PM) and Positive Large (PL) having centroids at − 1,-0.5,0,0.5,1 respectively. The MFs map the crisp values into fuzzy variables. The triangular MFs are chosen for this work due to its simplicity and adaptability in the tuning process [28].

The second module is the inference engine which comprises the rule base and database. Decision making is an inference control action from the rule base which is shown in Table 1.

The third module is the defuzzification, which converts the sum of fuzzy singleton outputs into an equivalent crisp value which is the output of FLC. The defuzzified output of FLC can be expressed as:

$$U_f = \frac{\sum_{j=1}^{25} \zeta_j Q_j}{\sum_{j=1}^{25} Q_j} \tag{6}$$

As shown in Section 4, the FO-Fuzzy-PID controller has superior performance when compared to FO-PID and conventional PID controllers. The crucial factor about the FLC is, its performance highly depends on its parameters (i.e. MFs and rule base). Without precise information about the system, the selection of parameters would not be appropriate. Hence, the designed FLC may not provide optimal performance over a wide range of operating conditions. To addresses the above problem, this paper proposes an adaptive FO-FLC-PID controller, in which MFs scaling factors and rule base weights are tuned in online according to operating conditions along with FO-PID parameters.

4 Proposed method (adaptive FO-FLC-PID controller)

In literature, there exist several approaches to tune the MFs scaling factors and rule base of a fuzzy logic controller for various engineering problems [29–31]. Several authors proposed FO-PID controllers as a solution to some engineering problems including LFC. However, no attempt has been made to combine both the techniques and inherit the merits of each technique by ignoring individual limitations in the process of resolving modern power system stability issues. Based on the requirements and complexities in frequency control of renewable penetrated power system, this paper proposes a novel adaptive FO-FLC-PID controller for an interconnected power system. Figure 7 depicts the block diagram of online tuning mechanism of the proposed controller. It can be observed that based on the ACE (which resembles the actual operating conditions of the system and feedback to the controller) and desired set point, the parameters of the proposed controller are tuned in online according to actual operating

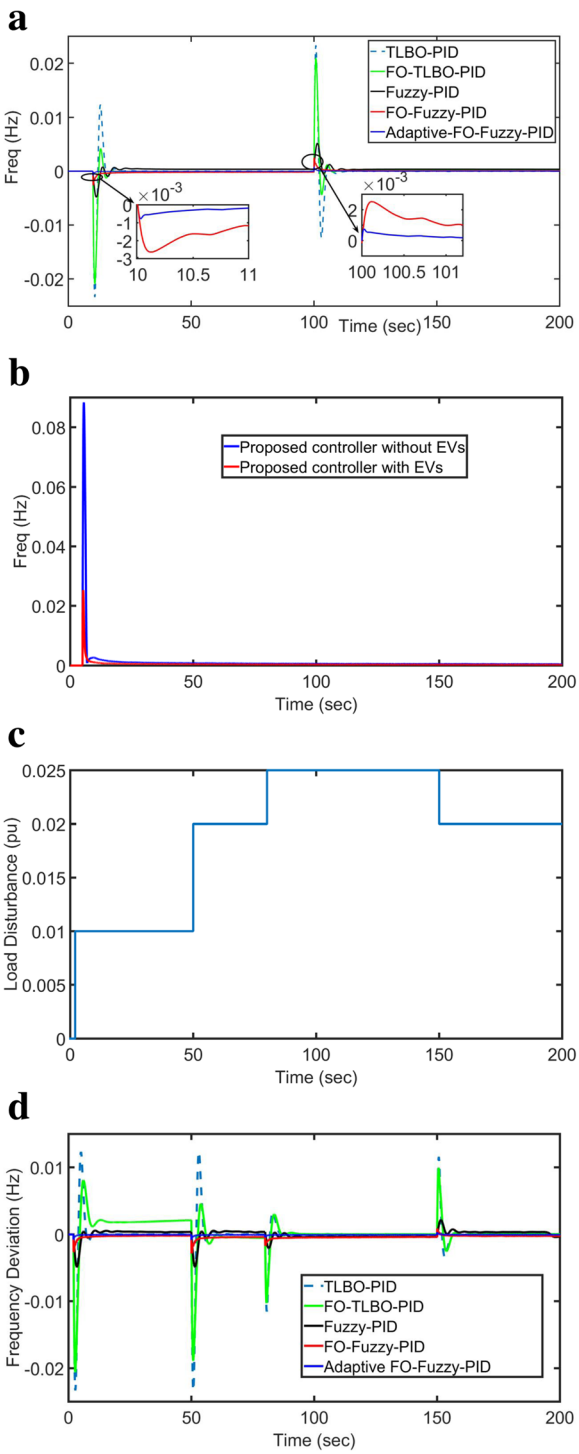

Fig. 9 **a** Case 1- Frequency deviation response, **b** Case 2 - Frequency deviation response, **c** Case - 3 Multistep Load deviations, **d** Case 3 - Frequency deviation response

Table 2 Comparative study of various controllers for case 1 & 2

Controller	Case 1				Case 3 at T = 150 s	
	For a load disturbance		Wind power disturbance			
	Peak Under shoot (Hz)	Settling Time (sec)	Peak Over shoot (Hz)	Settling Time (sec)	Peak Overshoot	Settling Time (sec)
TLBO-PID	−0.0235	20	0.024	21	0.0115	18
FO-TLBO-PID	−0.021	16	0.021	16	0.01	14
Fuzzy-PID	−0.005	15	0.0045	15	0.0022	10
FO-Fuzzy-PID	−0.0025	11	0.0025	11	0.001	5
Adaptive FO-Fuzzy-PID	**−0.001**	**5**	**0.001**	**5**	**0.0005**	**3**

conditions. The specific goal of ACE minimization through the proposed controller is attained by executing the following steps in online:

1) Tuning of fuzzy parameters (MFs scaling factors and rule weights)
2) Tuning of FO-PID controller.

In order to perform this task, a TLBO algorithm has been employed. The reason for selecting TLBO is, most of the meta-heuristic techniques like GA, PSO, GWO, and BHO, etc. highly depends on their own algorithm-specific parameters. Inappropriate choice of these parameters may lead the solution towards divergence. To overcome this problem, an algorithm-specific parameter free optimization technique (TLBO) is used in this paper. TLBO algorithm was introduced in 2012 by Dr.R.V.Rao, inspired from the teaching-learning process. This technique mimics the teaching-learning process in a classroom. It describes two phases of learning

a) Through teacher is known as teacher phase
b) Through the interaction of learners with other learners is known as the learner phase.

4.1 Teacher phase

In teacher phase, he tries to improve class mean result from a_1 to any other value a_2 depending on his capability called teaching factor (TF). At any iteration i, let us consider 'n' number of subjects (design variables), 'p' no of learners (population size (k = 1,2---p)). $M_{n,\ i}$ represents the total population mean of 'n^{th}' variable in 'i^{th}' iteration. The best of the population ($X_{total-kbest,\ i}$)considering all subjects together will be the best learner. According to this algorithm, the best learner is considered as the teacher. The mean_difference of each variable with respect to the teacher can be expressed as:

$$mean\_difference_{n,k,i} = rand()*\left[X_{n,kbest,i} - T_F M_{n,i}\right] \tag{7}$$

Where $X_{n,kbest,i}$ is the best learner who is considered as the teacher; rand = random number between [0–1]; T_F is a teaching factor which can be expressed as:

$$T_F = \text{Round}\left[1 + \text{ rand } () \ \{2\text{-}1\}\right] \tag{8}$$

T_F = 1 indicates no increase in the knowledge level of learner in a particular subject 'n'. T_F = 2 indicates the complete transfer of knowledge.

$$X'_{n,k,i} = X_{n,k,i} + mean\_difference_{n,k,i} \tag{9}$$

Where, $X'_{n,k,i}$ is the updated knowledge of each learner after teaching phase.

4.2 Learners phase

The second phase in this algorithm is the learner phase. In this phase, learners improve their knowledge by interacting among themselves. Select two learners in the

Table 3 Dynamic performance of the proposed controller with & without EVs

Controller	Case 2	
	Peak Over shoot (Hz)	Settling Time (sec)
Adaptive FO-Fuzzy-PID without EVs	0.088	27
Adaptive FO-Fuzzy-PID with EVs	0.025	13

Table 4 Uncertain parameters of the test system and PHEV aggregator

Parameters	Variation Range (in %)
M	−20
D	−10
T_{GT},T_{GH}	+ 10
R	+ 15
T_w	+ 15
T_{EV}	+ 50
R_{AG}	−50
K_{EV}	−30

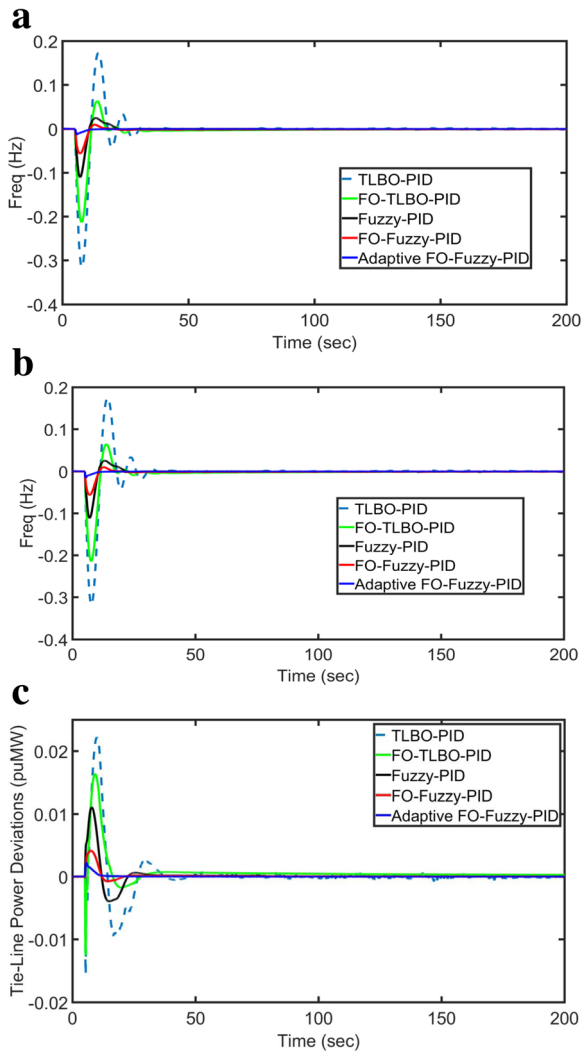

Fig. 10 Frequency deviation response of **a** area 1, **b** area 2 for scenario 2, **c** Tie-line power deviation

population A & B randomly such that $X'_{total_A,i} \neq X'_{total_B,i}$. Equation (10) describes how the learners transfer their knowledge between each other. Where $X'_{total_A,i}$ is the total fitness value of the learner in all subjects.

$$\begin{aligned} X''_{n,A,i} &= X_{n,A,i} + rand*\left(X'_{n,A,i} - X'_{n,B,i}\right); \\ &\text{if } X'_{n,B,i} < X'_{n,A,i} X''_{n,B,i} = X_{n,B,i} \\ &+ rand*\left(X'_{n,B,i} - X'_{n,A,i}\right); \\ &\text{if } X'_{n,A,i} < X'_{n,B,i} \end{aligned} \tag{10}$$

$X'_{n,A,i}$ denotes updated knowledge of Ath learner after learning phase.

The summarized steps for tuning the parameters of adaptive FO-FLC-PID controller with TLBO are given as follows:

Step 1: Initialize the population using $X_n = lb + rand * (ub - lb)$

Where,

lb=[**0 0 0 0 zeros (1,25)** 0 0 0 0 0]

ub=[**1 1 1 1 ones (1,25)** 5 5 1 5 1]

Fuzzy scaling Factors | Fuzzy Rule Weights | FO-PID Parameters

Step 2: Calculate the fitness of each learner (population) using the following fitness function

$$\begin{aligned} \text{ITAE} = \text{minimization of} \\ \int_0^{t_{sim}} t*(K_P*(|ACE_1| + |ACE_2|) + \frac{K_I}{S^\lambda} \\ *(|ACE_1| + |ACE_2|) + s^\mu \\ *K_D*(|ACE_1| + |ACE_2|))*\text{dt} \end{aligned} \tag{11}$$

Where, t_{sim} = total simulation time ($t_{sim} = 200$ *seconds*); t = time at which absolute sum of error samples are collected (t = 1,2,3---200 s)

Table 5 Comparative study of various controllers for scenario 2

Methods	Performance indices								
	Area 1			Area 2			Tie-line power deviation		
	PUS (Hz)	POS (Hz)	T_s (s)	PUS (Hz)	POS (Hz)	T_s(s)	PUS (puMW)	POS (puMW)	T_s(s)
TLBO-PID	−0.3	0.15	40	− 0.31	0.17	42	−0.015	0.025	55
FO-TLBO-PID	−0.21	0.08	36	−0.22	0.09	38	−0.012	0.016	49
Fuzzy-PID	−0.11	0.03	21	−0.11	0.035	23	−0.005	0.011	36
FO-Fuzzy-PID	−0.061	0.01	15	−0.057	0.012	17	−0.002	0.004	20
Adaptive FO-Fuzzy-PID	**−0.013**	**–**	**8**	**0.015**	**–**	**10**	**–**	**0.002**	**12**

PUS Peak undershoot, *POS*: Peak overshoot, T_s Settling time

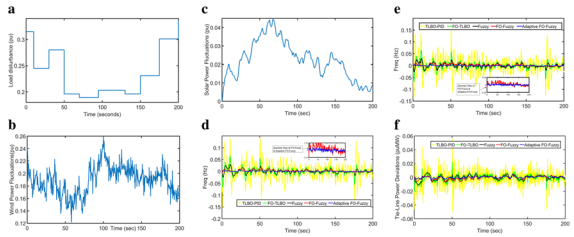

Fig. 11 **a** Load profile **b** Wind farm power deviations **c** solar power deviations; frequency deviation response of **d** area 1, **e** area 2, **f** Tie-line power flow deviation

Step 3: The best fitness one in the population is considered as the teacher. Calculate the mean of learners (population) in each subject (variable). Calculate mean_difference & T_F using following Eqs. (7) & (8).

Step 4: Update each learner's knowledge with the help of the teacher's knowledge using the Eq. (9).

Step 5: Each learner improves his/her knowledge by interacting with other learners according to Eq. (10).

Step 6: If the termination criteria is met (terminate either the tolerance value of ITAE reaches below 0.001 or the iteration count reaches 50), then display the optimal parameters of FLC and FO-PID controller, else return to step 2.

Figure 8 depicts the flow chart for the tuning process of proposed controller with TLBO algorithm.

5 Results and discussions

The adequacy of the proposed controller in frequency control under various scenarios is tested on the IEE Japan East 107-bus-30- machine power system. This system is recognized as a standard test system to assess the new control strategies with RES penetration. This test system is programmed and simulated in MATLAB 2015a environment. The parameters of the test system are listed in Appendix (A.1). The performance of the adaptive FO-FLC-PID controller is compared with other controllers in literature i.e., FO-FLC-PID, Fuzzy-PID, FO-PID, and TLBO- PID under various test scenarios. It is well known that the system response relies upon the parameters of these controllers, all the parameters are optimized by using TLBO algorithm.

5.1 Scenario 1

The objective of this scenario is to show the superiority of the proposed controller in improving the settling time and overshoots when compared with the other techniques available in the literature. To perform this task, three cases are considered in area 1 alone as an isolated area with EVs.

5.1.1 Case 1

In this case, a step change of 0.01 p.u.in load and wind power is applied at t = 10 & 100 s as a disturbance to the LFC in area 1. The frequency deviation response of various controllers are depicted in Fig. 9a.

5.1.2 Case 2

In this case, a step change of 0.1 p.u.in wind power is applied at t = 5 s as a disturbance to the LFC in area 1. This case is to demonstrate the dynamic performance of the system with the proposed controller, with & without PHEVs in frequency regulation. Figure 9b depicts the frequency deviation response of the system.

5.1.3 Case 3

In this case, a multi-step load deviation is applied as a disturbance to the LFC in area1. Figure 9c shows the multi-step load deviations. The frequency deviation response of various controllers is depicted in Fig. 9d.

From the Fig. 9a, b & d, it is observed that the dynamic performance is improved and the proposed LFC control scheme can eliminate the effect of load disturbance significantly when compared to other controllers. The dynamic performance of various controllers in cases 1 & 3 in terms of settling time and overshoot are listed

Table 6 Comparative study of various controllers for scenario 3

Controller	Area 1		Area 2		Tie-Line		ITAE
	PUS	POS	PUS	POS	PUS	POS	
TLBO-PID	−0.16	0.14	− 0.14	0.1625	−0.052	0.056	0.11
FO-TLBO	−0.07	0.06	−0.063	0.0635	−0.021	0.022	0.086
Fuzzy	−0.029	0.028	−0.026	0.0292	−0.011	0.008	0.0281
FO-Fuzzy	−0.008	0.01	−0.005	0.012	−0.006	0.005	0.00985
Adaptive FO-Fuzzy	**−0.004**	**0.005**	**−0.0001**	**0.0045**	**−0.002**	**0.0025**	**0.0061**

Table 7 Optimized parameters of various controllers in area1

Optimized parameters of various controllers in area1

Controller Parameters	TLBO-PID	FO-TLBO-PID	Fuzzy-PID	FO-Fuzzy-PID	Adaptive FO-Fuzzy-PID
K_e	-	-	1	0.1413	0.1060
K_{ce}	-	-	1	1	0.2213
K_u	-	-	1	0.672	0.431
K_P	4.4611	4.6969	2.4133	0.98247	1.5099
K_I	4.3982	2.4409	4.4003	3.0206	3.0119
K_D	3.3559	2.4587	3.3571	3.9201	3.3571
λ	-	0.773	-	0.7175	0.4261
μ	-	0.6078	-	0.6935	0.0530
d^n/dt^n	-	-	1	0.5678	0.1672

In the proposed controller, in addition to above parameters rule base weights also optimized as shown in Table 8

in Table 2. The dynamic performance of the proposed controller with and without EVs (case 2) is listed in Table 3.

5.2 Scenario 2

The objective of this scenario is to show the robustness of the proposed controller against parametric uncertainties in the system as well as PHEV aggregator. The percentage changes in the parameters of the system and PHEV aggregator are displayed in Table 4.

In this scenario, a step change of 0.05 p.u.in load is applied as a disturbance to the LFC in area 1 along with parametric uncertainties as mentioned in Table 4. The frequency deviation response of area 1, area 2 and tie-line power deviations with various controllers are shown in Fig. 10a-c. The dynamic performance of various controllers for scenario 2 is listed in Table 5.

From the scenario 2, it is clear that the proposed adaptive FO-Fuzzy-PID controller improves the dynamic response of the system significantly over other methods. Moreover, the simulation results reveal that the proposed approach is more robust to parametric uncertainties over other controllers. On the other hand, the TLBO-PID, FO-TLBO-PID and fuzzy PID controllers have large overshoots and more settling time under the circumstances as mentioned in scenario2.

5.3 Scenario 3

In this scenario, it is assumed that there are load changes and wind power changes in area 1 and solar power changes in area 2. The wind power data is extracted from GAMESA company WTG data sheet [32], solar power data from [33]. Figure 11a-c illustrates the load, wind power and solar power changes in area 1 and area 2 respectively. Figure 11d & e represents the frequency deviation response in area 1 and area 2. Figure 11f depicts the tie-line power flow deviations between area1 and area 2.

Figure 11d-f reveal that the proposed controller has minimized the frequency and tie-line power deviations effectively with a lesser magnitude of the error and overshoots with respect to other controllers. The ITAE (error value) performance criteria of various controllers for scenario 3 is listed in Table 6. The optimized gains of various controllers are given in Table 7. The rule weights of the proposed controller are listed in Table 8. Figure 12 shows the convergence characteristics of the various controllers for scenario 3.

5.4 Scenario 4

Finally, to explore the robustness of the proposed controller at the next level, the PHEV aggregator is disconnected from the grid at t = 100 s in scenario 4. For analysis purpose, only a single area (i.e., area

Table 8 Rule weights of the proposed adaptive FO-fuzzy controller

Rule 1	**Rule 2**	**Rule 3**	**Rule 4**	**Rule 5**	**Rule 6**	**Rule 7**	**Rule 8**	**Rule 9**	**Rule 10**
0.6472	0.5551	0.5314	0.6093	0.9123	0.4630	0.8989	0.6900	0.4128	0.332
Rule 11	**Rule 12**	**Rule 13**	**Rule 14**	**Rule 15**	**Rule 16**	**Rule 17**	**Rule 18**	**Rule 19**	**Rule 20**
0.3977	0.7608	0.0622	0.4265	0.5241	0.5377	0.4644	0.6855	0.4749	0.5987
Rule 21	**Rule 22**	**Rule 23**	**Rule 24**	**Rule 25**					
0.7433	0.6897	0.2391	0.3964	0.3579					

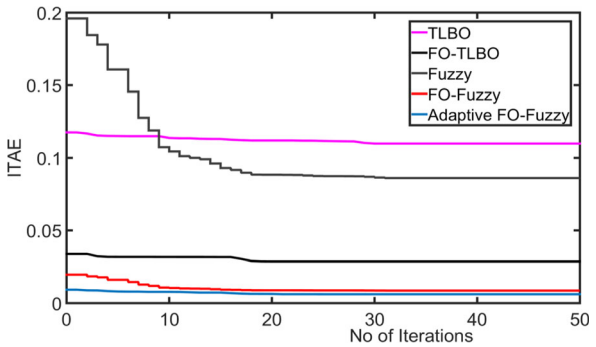

Fig. 12 Optimized parameters of various controllers in area1

1 as an isolated area) is considered. The same load along with wind and solar power disturbances are considered simultaneously in area1 as shown in Fig. 11a-c.

Figure 13 illustrates the simulation results for this scenario. It also shows that the proposed controller improves the frequency response of the system in comparison to other controllers in the literature, especially where the overshoots are concerned. Certainly, from Fig. 13, despite parametric uncertainties and EV aggregator disconnection, the proposed controller shows its supremacy over the other four controllers. As it can be noticed, the TLBO-PID, FO-TLBO-PID, and Fuzzy-PID controllers unable to provide acceptable performance in scenario 4. FO-Fuzzy-PID controller and proposed adaptive FO-Fuzzy-PID controller have provided an agreeable performance in this scenario. In this duo, the proposed controller shows its superiority in error and overshoot reduction in comparison with FO-Fuzzy-PID controller.

6 Conclusion

In this work, a novel adaptive FO-FLC-PID controller is proposed for frequency control of an interconnected power system with RES penetration. In order to improve the robustness against RES intermittencies and load disturbances, the proposed controller is designed at two levels, i.e., Fuzzy and FO-PID control levels. Since the FLC's performance depends on its MFs and rule base, both are tuned by using TLBO algorithm along with FO-PID parameters. This proposed approach improves the performance of the LFC with low computation burden and complexity. Moreover, the proposed controller was found adaptive enough to handle the uncertainty in the loads, RES power output and system parameters. The simulation results from the four scenarios validate that the proposed controller is able to minimize the frequency deviations significantly over the TLBO-PID, FO-TLBO-PID, fuzzy PID, FO-FLC-PID controllers.

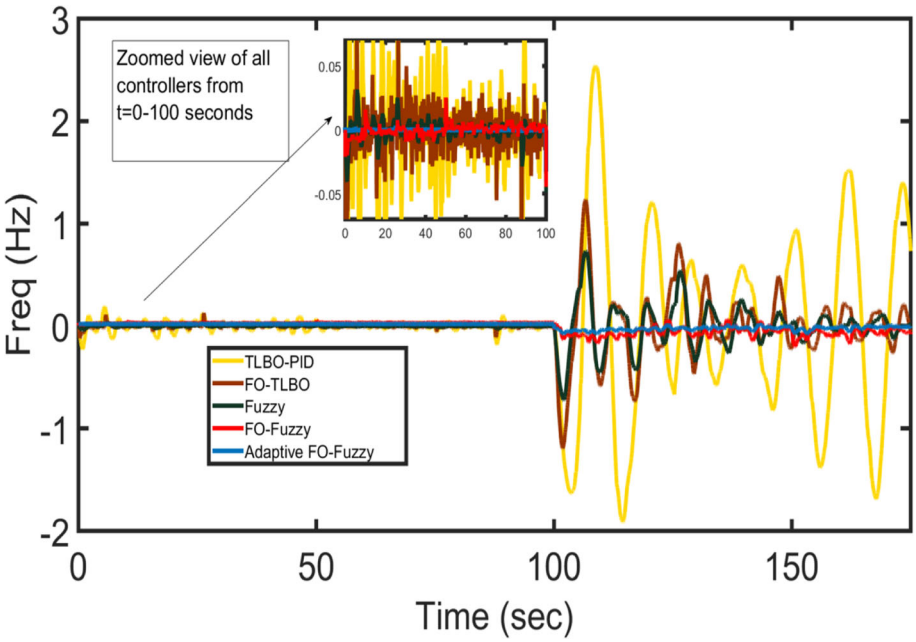

Fig. 13 ITAE performance curve for scenario 3

7 Appendix

7.1 IEE-Japan-East-107-bus data

$$M_1 = 8.85\text{puMW-s}^2, D_1, D_2 = 0.04\ \text{puMW/Hz}, M_2 = 9.2, R_1, R_2 = 2.4\ \text{Hz/puMW}, \beta_1, \beta_2 = 0.4566\ \text{puMW/Hz}, T_{12} = 5$$

7.2 Thermal generator data

$$T_{GT} = 0.2\ \text{s}; T_{TT} = 0.3\ \text{s}; T_{r1} = 10\ \text{s}; K_{r1} = 0.333; K_1, K_2, K_3 = 0.85, 0.095, 0.92; K_{ib} = 0.03; C_b = 200; T_{ib} = 26\ \text{s}; T_{rb} = 69\ \text{s}; T_f = 10\ \text{s}; R_T = 2.4\ \text{Hz/puMW}.$$

7.3 Hydro generator data

$$T_{GH} = 0.1\ \text{s}; T_1 = 0.513\ \text{s}; T_2 = 10\ \text{s}; T_w = 1\ \text{s}; R_H = 2.4\ \text{Hz/puMW}.$$

7.4 PHEV data

$$\Delta f_u = \text{Upper frequency dead band} = 10\ \text{mHz}, \Delta f_l = \text{Upper frequency dead band} = -10\ \text{mHz}, T_{EV,i} = 0.1, R_{av} = 2.4\ \text{Hz/puMW}, N_{EV} = 40,000\ (\text{output of each EV} \pm 10\ \text{kw}), K_{EV,i}\ (\text{average}) = 0.55, SOC_1 = 0.2, SOC_2 = 0.25, SOC_3 = 0.85\ \text{and}\ SOC_4 = 0.9$$

Acknowledgments
Authors would like to thank the National Institute of Technology Warangal (NITW) for providing the necessary research facilities.

Authors' contributions
AA analyzed and interpreted the modeling and simulation of the test system and controller. SN provided the idea and other technical guidance required for completion of the work. He also prepared the final draft of the manuscript. Both authors have read and approved the final manuscript.

Authors' information
Anil Annamraju was born in Nellore, India. He received his B.Tech degree in Electrical and Electronics Engineering from Jawaharlal Nehru Technological University, Kakinada, India, in 2010 and M.Tech degree in Power systems from University of Calicut, India, in 2013. Currently, He is working as research scholar in the Electrical Engineering department, National Institute of Technology, Warangal, India. His research interests include Microgrid technologies, Power system stability, operation and Control with Intelligent Techniques.
Srikanth Nandiraju received his B.Tech degree in Electrical and Electronics Engineering from Osmania University, Hyderabad, India, in 1988 and M.Tech degree in Power systems from REC, Warangal, India, in 1998. He received his Ph.D. degree from National Institute of Technology, Warangal, India, in 2006. Since 1989, he is working as faculty in various positions. Currently, he is working as associate professor in the Electrical Engineering department, National Institute of Technology, Warangal, India. He is a member of IEEE and Institute of Engineers (India). He published over 40 research papers in journals and conferences. His research interests include power system stability, operation and control, application of intelligent techniques to Microgrid problems, Real time control of power system, HVDC and FACTS.

Funding
Not applicable.

Availability of data and materials
Data sharing not applicable to this article as no data were generated or analyzed during the study.

Competing interests
The authors declare that they have no competing interests.

Received: 7 January 2019 Accepted: 31 July 2019
Published online: 30 August 2019

References

1. Bevrani, H., Ghosh, A., & Ledwich, G. (2010). Renewable energy sources and frequency regulation: survey and new perspectives. *IET Renewable Power Generation, 4*(5), 438–457.
2. Kouba, N., Mohamed, M., Mourad, H., & Mohamed. (2016). LFC enhancement concerning large wind power integration using new optimized PID controller and RFBs. *IET Generation, Transmission & Distribution, 10*(16), 4065–4077.
3. Hill, C., Such, M. C., Chen, D., et al. (2012). Battery energy storage for enabling integration of distributed solar power generation. *IEEE Transactions on Smart Grid, 3*(2), 850–857.
4. Ravi, S., Kalyan, C., et al. (2016). Impact of energy storage system on load frequency controlfor diverse sources of interconnectedpower system in deregulated power environment. *International Journal of Electrical Power & Energy Systems (Elsevier), 79*, 11–26.
5. Robert, C., et al. (2011). The impact of plug-in hybrid electric vehicles on distribution networks: A review and outlook. *Renewable and Sustainable Energy Reviews, 15*, 544–553.
6. Chao, P., Jianxiao, Z., Lian, L. (2017). Dispatching strategies of electric vehicles participating in frequency regulation on power grid: A review. *Renewable and Sustainable Energy Reviews, 68*(1), 147–152. https://doi.org/10.1016/j.rser.2016.09.133.
7. Ota, Y., Taniguchi, H., Nakajima, T., et al. (2012). Autonomous distributed V2G (vehicle-to-grid) satisfying scheduled charging. *IEEE Transactions on Smart Grid, 3*(1), 559–564.
8. Liu, H., Hu, Z., Song, Y., et al. (2015). Vehicle-to-grid control for supplementary frequency regulation considering charging demands. *IEEE Transactions on Power Systems, 30*(6), 3110–3119.
9. Vachirasricirikul, S., & Ngamroo, I. (2014). Robust LFC in a smart grid with wind power penetration bycoordinated V2G control and frequency controller. *IEEE Transactions on Smart Grid, 5*(1), 371–380.
10. Qudaih, Y., Moukhtar, I., Mohamed, T. H., et al. (2016). Parallel PI/CDM frequency controller to support V2G plan for microgrid. *Energy Procedia, 100*, 342–351.
11. Pahasa, J., & Ngamroo, I. (2017). Simultaneous control of frequency fluctuation and battery SOC in a smart grid using LFC and EV controllers based on optimal MIMO-MPC. *Journal of Electrical Engineering and Technology, 12*(1), 1921–1931.
12. Thanh, P., et al. (2016). Integration of electric vehicles for load frequency output H∞ control of smart grids. *IET Generation, Transmission & Distribution, 10*(13), 3341–3352.
13. Hongjie, J., et al. (2018). Coordinated control for EV aggregators and power plants in frequency regulation considering time-varying delays. *Applied Energy, 210*, 1363–1376.
14. Falahati, S., et al. (2016). Grid frequency control with electric vehicles by using of an optimized fuzzy controller. *Applied Energy, 178*, 918–928.
15. Debbarma, S., & Dutta, A. (2017). Utilizing electric vehicles for LFC in restructured power systems using fractional order controller. *IEEE Transactions on Smart Grid, 8*(6), 2554–2564.
16. Saha, A., et al. (2018). Performance analysis of combination of ultra-capacitor and superconducting magnetic energy storage in a thermal-gas AGC system with utilization of whale optimization algorithm optimized cascade controller. *Journal of Renewable and Sustainable Energy, 10*, 014103.
17. Khezri, R., Oshnoei, A., et al. (2018). Coordination of heat pumps, electric vehicles and AGC for efficient LFC in a smart hybrid power system via SCA-based optimized FOPID controllers. *Energies, 11*, 420.
18. Datta, M., & Senjyu, T. (2013). Fuzzy control of distributed PV inverters/energy storage systems/electric vehicles for frequency regulation in a large power system. *IEEE Transactions on Smart Grid, 4*(1), 479–488.

19. Khoonab, et al. (2018). Load frequency control in microgrids based on a stochastic non-integer controller. *IEEE Transactions on Sustainable Energy, 9*(2), 853–861.
20. Liu, T., Hill, D., & Zhang, C. (2016). Non-disruptive load-side control for frequency regulation in power systems. *IEEE Transactions on Smart Grid, 7*(4), 2142–2153.
21. Anil, A., & Srikanth, N. (2018). Robust frequency control in an autonomous microgrid- a two-stage adaptive fuzzy approach. *Electric Power Components and Systems, 46*(1), 83–94.
22. Rao, R., et al. (2016). *Teaching-learning based optimization algorithm and its engineering applications* (1st ed.). Springer. https://doi.org/10.1007/978-3-319-22,732-0.
23. Kundur, P. (1994). *'Power system stability and control*. New York: McGraw-Hill.
24. Wen, T., et al. (2017). Load frequency control of power system with non-linearities. *IET Generation, Transmission & Distribution, 11*(17), 4307–4313.
25. Izadkhast, et al. (2015). An aggregate model of plug-in electric vehicles for primary frequency control. *IEEE Transactions on Smart Grid, 30*(3), 1475–1482.
26. Monje, C., et al. (2010). Numerical issues and MATLAB Implementations for Fractional-order control Systems. In *Fractional-order systems and controls* (1st ed.). London: Springer-Verlag. https://doi.org/10.1007/978-1-84996-335-0.
27. Swati, S., et al. (2014). Fractional order PID controller for load frequency control. *Energy Conversion & Management, 85*, 343–353.
28. Mudi, R., & Pal, N. (1999). A robust self-tuning scheme for PI and PD-type fuzzy controllers. *IEEE Transactions on Fuzzy Systems, 7*(1), 2–16.
29. Khooban, M., et al. (2016). A robust adaptive load frequency controlfor microgrids. *ISA Transactions, 65*, 220–229.
30. Arya, Y. (2017). AGC performance enrichment of multi-source hydrothermal gas power systems using new optimized FOFPID controller and redox flow batteries. *Energy, 127*, 704–715.
31. Sahu, B., Pati, S., et al. (2014). Hybrid differential evolution particle swarm optimisationoptimised fuzzy proportional integral derivative controller for automatic generation control of interconnected power system. *IET Generation, Transmission & Distribution, 8*(11), 1789–1800.
32. WINDPOWER. Available at https://www.thewindpower.net/turbine_en_42_gamesa_g52-850.php. Accessed 12 NoV 2017.
33. El-Fergany, A. A., & Elhameed, M. A. (2016). Efficient frequency controllers for autonomous two-area hybrid microgrid system using social-spider optimiser. *IET Generation, Transmission & Distribution, 11*(3), 637–648.